Loss of the E3 ubiquitin ligase LRSAM1 sensitizes peripheral axons to degeneration in a mouse model of Charcot-Marie-Tooth disease

Laurent P. Bogdanik[1], James N. Sleigh[1,2], Cong Tian[1,3], Mark E. Samuels[4], Karen Bedard[5], Kevin L. Seburn[1] and Robert W. Burgess[1,3,*]

SUMMARY

Charcot-Marie-Tooth disease (CMT) is a clinically and genetically heterogeneous condition characterized by peripheral axon degeneration with subsequent motor and sensory deficits. Several CMT gene products function in endosomal sorting and trafficking to the lysosome, suggesting that defects in this cellular pathway might present a common pathogenic mechanism for these conditions. LRSAM1 is an E3 ubiquitin ligase that is implicated in this process, and mutations in *LRSAM1* have recently been shown to cause CMT. We have generated mouse mutations in *Lrsam1* to create an animal model of this form of CMT (CMT2P). Mouse *Lrsam1* is abundantly expressed in the motor and sensory neurons of the peripheral nervous system. Both homozygous and heterozygous mice have largely normal neuromuscular performance and only a very mild neuropathy phenotype with age. However, *Lrsam1* mutant mice are more sensitive to challenge with acrylamide, a neurotoxic agent that causes axon degeneration, indicating that the axons in the mutant mice are indeed compromised. In transfected cells, LRSAM1 primarily localizes in a perinuclear compartment immediately beyond the Golgi and shows little colocalization with components of the endosome to lysosome trafficking pathway, suggesting that other cellular mechanisms also merit consideration.

INTRODUCTION

Hereditary sensory and motor neuropathies (HSMNs), or Charcot-Marie-Tooth diseases (CMTs), are a genetically heterogeneous set of conditions that lead to peripheral axon degeneration and distal motor and sensory dysfunction. Genetically, there are over 40 loci associated with CMTs, and inheritance can be dominant, recessive or X-linked (http://www.molgen.ua.ac.be/CMTMutations/Home/IPN.cfm). Demyelinating, or type 1, neuropathies are increasingly well understood and are often associated with genes expressed by Schwann cells encoding the structural proteins of myelin. Axonal, or type 2, neuropathies are less well understood, although themes including the axonal cytoskeleton, axonal transport and mitochondrial function are emerging, based on disease-associated genes identified to date.

Another emerging pathway in peripheral neuropathy is endosomal sorting and targeting to the lysosome (Fig. 1A). The SH3TC2 protein (SH3 domain and tetratricopeptide repeat domain 2), implicated in CMT4C, colocalizes with RAB11 on recycling endosomal vesicles (Senderek et al., 2003; Roberts et al., 2010; Stendel et al., 2010). The small integral membrane protein of the lysosome/late endosome (SIMPLE or LITAF) is associated with both early and late endosomes, and mutations in *SIMPLE* cause CMT1C (Moriwaki et al., 2001; Street et al., 2003; Lee et al., 2011). SIMPLE also associates with tumor suppressor gene 101 (TSG101) (Shirk et al., 2005), a component of the ESCRT1 complex (endosomal sorting complex required for transport) that is involved in the formation of multivesicular bodies (MVBs) and trafficking from the late endosome to the lysosome (Hanson et al., 2009; Raiborg and Stenmark, 2009). FIG4, a phosphatidylinositol (3,5)-bisphosphate (PI3,5P2) phosphatase, is also involved in the formation of MVBs, and mutations in *FIG4* cause both peripheral neuropathy and motor neuron disease (Chow et al., 2007; Zhang et al., 2007; Chow et al., 2009). RAB7 is a small GTPase, the only RAB protein known to be associated with vesicles targeted to the lysosome, and mutations in *RAB7* cause CMT2B (Verhoeven et al., 2003). Despite the apparent importance of the endosomal sorting pathway in CMT and mechanistic commonalities, it should be noted that some of these mutations cause demyelinating neuropathies and might function in Schwann cells (SH3TC2, SIMPLE), whereas others cause axonal neuropathies and might function in neurons (RAB7, FIG4). Furthermore, the functions of these proteins in endosomal sorting and lysosomal targeting are poorly understood.

Recently, mutations in *LRSAM1* (leucine-rich repeat and sterile alpha motif containing 1) have been reported in axonal neuropathy, CMT2P (OMIM 614436) (Guernsey et al., 2010; Weterman et al., 2012; Nicolaou et al., 2012). In a Canadian pedigree, a truncating frame shift in *LRSAM1* results in an apparently null allele with no

[1]The Jackson Laboratory, Bar Harbor, ME, 04609, USA
[2]MRC Functional Genomics Unit, Department of Physiology, Anatomy and Genetics, University of Oxford, South Parks Road, Oxford, OX1 3QX, UK
[3]Graduate School of Biomedical Sciences, The University of Maine, Orono, ME 04469, USA
[4]Department of Medicine, Montreal University, Montreal, Quebec, H3T 1C5, Canada
[5]Department of Pathology, Dalhousie University, Halifax, Nova Scotia, B3H 4R2, Canada
*Author for correspondence (Robert.burgess@jax.org)

TRANSLATIONAL IMPACT

Clinical issue

Charcot-Marie-Tooth diseases (CMTs) are a genetically heterogeneous group of neuropathies that affect the peripheral nervous system. Over 40 loci have been linked with CMTs, and numerous disease-causing mutations have been identified. However, the mechanisms underlying axonal Charcot-Marie-Tooth disease type 2 (CMT2) remain poorly understood. Recently, mutations in *LRSAM1* were linked with axonal neuropathies that are clinically similar to CMT2. The *LRSAM1* gene encodes an E3 ubiquitin ligase that is hypothesized to interact with proteins involved in endosome to lysosome trafficking, a pathway that has recently been implicated in the pathogenic mechanism underlying some CMTs.

Results

To test the hypothesis that loss of LRSAM1 function and defects in endosomal sorting can lead to CMT2, the authors generated a mouse model of *LRSAM1*-associated neuropathy. The model was created by introducing loss-of-function mutations in the mouse *Lrsam1* gene using gene trap embryonic stem (ES) cells. Using *lacZ* reporter expression analysis, the authors show that *Lrsam1* is expressed at a high level in peripheral motor and sensory neurons. As expected, mice that are homozygous for the gene trap insertion produced no detectable LRSAM1 protein. These mice are reported to be generally healthy and to show only mild symptoms of peripheral neuropathy. However, the peripheral axons in homozygote mice exhibited a greater sensitivity to the neurotoxic effects of acrylamide, indicating that the axons are more susceptible to degeneration. The authors then examined the subcellular localization of LRSAM1 in transfected cells, and found that the protein localizes immediately surrounding a marker of the Golgi complex, and does not colocalize with other components of the endosome to lysosome sorting pathway.

Implications and future directions

The mice generated in this study provide an ideal model for the investigation of LRSAM1 function in Charcot-Marie-Tooth disease. Tissues from these mice will be useful for identifying potential substrates of LRSAM1. Based on the relatively mild phenotype observed, the authors suggest that mutations in *LRSAM1* might sensitize peripheral neurons to the effects of other mutations or environmental toxicities. The poor colocalization of LRSAM1 with other components of the endosome to lysosome sorting pathway suggests that additional cellular functions should be investigated as potential pathogenic mechanisms in LRSAM1-associated peripheral neuropathy.

detectable protein and causes a recessive axonal neuropathy (Guernsey et al., 2010). Patients present in young adulthood with distal muscle wasting, sensory deficits and electrophysiological signs consistent with CMT type 2. In a Dutch pedigree with a similar clinical presentation, a frameshift mutation in the final exon of *LRSAM1* alters the C-terminal coding sequence and causes a dominant polyneuropathy (Weterman et al., 2012). A similar mutation was found in a Sardinian pedigree with autosomal dominant axonal CMT, in which a splicing mutation results in a frame shift affecting the C-terminus of the protein (Nicolaou et al., 2012). Furthermore, knockdown of *Lrsam1* in zebrafish results in a defect in the fasciculation and targeting of motor axons, consistent with an important role for *Lrsam1* in the developing peripheral nervous system (Weterman et al., 2012).

LRSAM1 is an E3 ubiquitin ligase that is also called RIFLE or TAL1 (TSG101-associated ligase 1). In addition to four leucine-rich repeats, a sterile alpha motif and a C-terminal zinc finger ring domain, the protein contains two coiled-coil domains (CC) and two Pro-(Ser/Thr)-Ala-Pro (PTAP) tetrapeptide motifs (Fig. 1B). The second CC and the PTAP domains have been reported to bind

to TSG101 (Amit et al., 2004). TSG101 is the best-characterized substrate for LRSAM1, and LRSAM1 expression can influence TSG101 levels, which are crucial for its proper function (Li et al., 2003; Amit et al., 2004; McDonald and Martin-Serrano, 2008). Therefore, it is an attractive hypothesis to associate LRSAM1 in endosomal sorting and lysosomal targeting along with TSG101 and other CMT proteins such as SIMPLE.

Here we describe mutations in the mouse *Lrsam1* gene, which is strongly expressed in peripheral neurons. Mutant mice have mild neuromuscular junction and axonal defects, but are generally healthy unless challenged with the neurotoxic agent acrylamide, for which they show greater sensitivity and more rapid motor axon degeneration than control mice. In examining the subcellular localization of LRSAM1 in transfected cells, we found LRSAM1 labeling of puncta in the cytoplasm, but most labeling was found just beyond GM130, a marker of the Golgi complex. A similar localization was not observed with another cytoplasmic control protein in the same assay. There was also little colocalization with CD63 in late endosomes, EEA1 in early endosomes, or with TSG101. Therefore, although the endosomal/lysosomal sorting pathway might be involved in *LRSAM1*-associated and other neuropathies, other substrates of LRSAM1 and other cellular mechanisms should also be investigated.

RESULTS

Gene trap mutations in *Lrsam1*

To create an animal model of CMT2P and to determine whether the human disease is consistent with a loss of LRSAM1 function, or possibly a more complicated mechanism given the similar disease associated with both dominant and recessive-null human *LRSAM1* mutations, we generated loss-of-function mutations in mice using available gene trap embryonic stem (ES) cell strains. The mouse *Lrsam1* gene consists of 25 exons (26 if an additional 5′ non-coding exon is included), and two gene trap insertions generated by Bay Genomics in intron 21 (*RRK239*) and intron 22 (*RRK461*) were obtained (Fig. 1C). The exact positions of the insertions were determined by PCR and sequencing using *Lrsam1* forward and reverse primers in the gene trap vector (see Materials and Methods). Each ES cell line was reanimated by standard blastocyst injection, the mutations passed through the germline of subsequent chimeras and breeding colonies established.

The impact of the *Lrsam1* gene trap alleles on LRSAM1 protein levels was determined by western blotting (Fig. 1D). A mouse antibody raised against human LRSAM1 was used to probe a blot of spinal cord lysates prepared from wild-type, heterozygous and homozygous *Lrsam1* littermate mice. A single specific band of the predicted size (84 kDa) was detected in control samples and at reduced levels in samples from *Lrsam1^{RRK461}* heterozygous mice, but was undetectable in *RRK461* homozygotes. The predicted size of LRSAM1 was confirmed by blotting cell lysates from COS7 cells transfected with an *Lrsam1* cDNA (rLRSAM1, including C-terminal MYC and 6X-His tags). The lower molecular weight bands are non-specific immunoglobulins from the tissue lysate detected by the anti-mouse Ig secondary antibody. A GAPDH loading control confirmed equal loading of the samples. A second identical blot was probed with a rabbit anti-LRSAM1 antibody to detect possible alternative or truncated translation products in the gene trap mice. The epitope of this antibody (shown in Fig. 1C) is
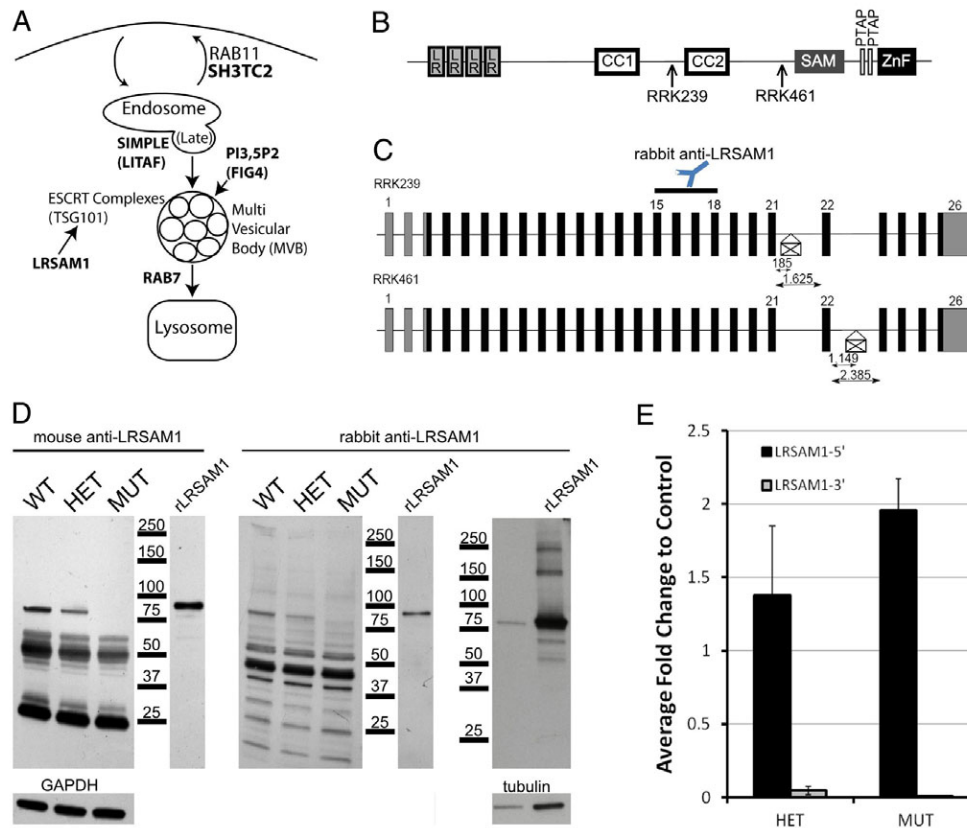
Fig. 1. The endosome to lysosome pathway and *Lrsam1* mutations in mice. (A) Schematic of the endosome to lysosome pathway. Proteins are endocytosed from the plasma membrane and either recycled back to the membrane or transited through the endosomal pathway. From the late endosome, multivesicular bodies are targeted to the lysosome for degradation. The formation of multivesicular bodies requires the ESCRT complexes for vesicle scission and the proper membrane composition of PI3,5P2. Key proteins that function in this pathway and also cause CMT disease when mutated are shown in bold. (B) Representation of the protein domains of LRSAM1. From the N-terminus to the C-terminus, LRSAM1 contains four leucine-rich repeats (LR), two coil-coiled domains (CC), the sterile-alpha motif (SAM), two PTAP domains and a zinc-finger motif of the RING type (ZnF). (C) Gene-trap alleles of the mouse *Lrsam1*. Representation of the *Lrsam1* gene structure and localization of the *RRK239* and *RRK461* gene-trap insertions. Exons are represented by black boxes. The diagram is not to scale. The intron sizes and positions of the insertions within the introns are shown. (D) Anti-LRSAM1 western blots on mouse spinal cord lysates and COS7 cells transfected with the *Lrsam1* cDNA. Samples were prepared from wild-type, heterozygous and homozygous mice for the *RRK461* gene trap insertion. A specific band of the expected size for LRSAM1 (84 kDa) was detected in wild-type samples and this size was consistent with recombinant protein expressed in COS7 cells (rLRSAM1). This band was reduced in heterozygotes and below detection in homozygotes. Blots were probed with either mouse anti-LRSAM1 (left panels) or rabbit anti-LRSAM1 (right panels) with similar results. The anti-mouse secondary antibody also recognized nonspecific immunoglobulin bands from the tissue whereas the rabbit anti-LRSAM1 antibody recognized a number of nonspecific background bands. With longer exposures, higher molecular weight bands were also detected in transfected COS7 cells (right panel, right lane), but not in untransfected cells. GAPDH (left lane) and tubulin were used as loading controls. (E) qRT-PCR on spinal cord extracts with primer pairs recognizing amplicons either upstream (5′) or downstream (3′) of the insertions. Relative transcript abundance in the heterozygotes (HET) and homozygote mutants. (MUT) for *Lrsam1^RRK461^* compared with wild-type mice (set at 1.0) is indicated. Error bars represent the confidence interval of the fold-change. *n*=7 for HET and 5 for MUT.

upstream of the gene trap insertion sites. Despite higher background, the blot again showed a band of 84 kDa that was reduced in heterozygous *RRK461* mice and eliminated in homozygous mice. Given the background bands, the ability of this antibody to detect LRSAM1 was again confirmed in COS7 cells transfected with the *Lrsam1* cDNA, where it very specifically recognized a single band of the correct size. With longer exposures, additional high molecular weight bands were detected in transfected cells, possibly indicating the multimerization of recombinant LRSAM1. However, we did not detect higher molecular weight species in tissue lysates, even under non-reducing conditions (Fig. 1D and not shown), so their presence *in vivo* remains speculative. Immunoblotting of *RRK239* tissue showed a

similar profile, but some persistent protein was present in homozygous mice (not shown). Because the *RRK461* insertion appeared to be the more complete loss-of-function, we performed our subsequent analyses in that line unless specifically noted.

Quantitative RT-PCR (qRT-PCR) further demonstrated the loss of *Lrsam1* expression. Using an amplicon upstream of the gene trap insertion, little change or an increase in expression level was observed, as anticipated for the production of a fusion transcript between *Lrsam1* and the gene trap *lacZ* reporter and consistent with analysis of other gene trap insertion knockout mouse strains (Burgess et al., 2000; Fuerst et al., 2009). However, qRT-PCR analysis using an amplicon downstream of the insertion revealed a decrease in mRNA levels to the threshold of detection (Fig. 1E). A marked

drop in *Lrsam1* transcript levels was also observed in *RRK461* heterozygous mice. Thus, both gene trap lines effectively reduce *Lrsam1* expression, but homozygosity for *RRK461* reduces expression to below detectable levels in analysis of both protein and mRNA.

Lrsam1 expression in the mouse

We next examined the expression pattern of *Lrsam1* in the mouse using the *lacZ* reporter incorporated into the gene trap vector. In spinal cord cross-sections, robust β-galactosidase (βGal) activity was detected in motor neurons in the ventral horn (Fig. 2A,B). This pattern was consistent in both the *RRK461* and *RRK239* lines. In addition, βGal activity was detected in the cell bodies of peripheral sensory neurons in the dorsal root ganglia (DRGs) (Fig. 2C). Some βGal activity was also present in the brain stem, consistent with cranial nerve motor nuclei (not shown). No βGal activity was detectable in other parts of the nervous system, in muscle of mice with the gene trap insertions, or in the spinal cord or DRGs of wild-type mice (not shown). To examine the possibility of a developmental role for *Lrsam1*, we used *in situ* hybridization to probe transverse sections from embryonic day 15.5 (E15.5) embryos for *Lrsam1* expression (Fig. 2D). *Lrsam1* expression was detected at a low level in many tissues and was enriched in the dorsal root ganglia and spinal cord, consistent with expression reported in human fetal samples (Weterman et al., 2012). The position of motor neurons and the specificity of the technique were demonstrated by hybridizing adjacent sections with a probe recognizing choline acetyltransferase (Fig. 2E). We examined the spinal cord, cerebellum and hippocampus by hematoxylin and eosin histology and ubiquitin staining to detect cellular stress or death in the homozygous mutant mice, but no

Fig. 2. Expression of *Lrsam1* in the nervous system. (A-C) Gene-trap-derived β-galactosidase activity reporting *Lrsam1* expression pattern was revealed by cytochemistry in the adult ventral spinal cord motoneurons of the *RRK239* (A), and *RRK461* (B) gene trap lines, and in wholemount dorsal root ganglia of the *RRK461* line (C). No β-galactosidase activity was detected in wild-type mice processed in parallel (not shown). (D) *Lrsam1 in situ* hybridization on embryonic (15.5 days post-fertilization) transverse sections revealed broad low-level expression with particular enrichment in the dorsal root ganglion (arrow) and throughout the spinal cord. (E) The position of ventral horn motor neurons and the specificity of probes are demonstrated by *in situ* hybridization with choline acetyltransferase (Chat). Scale bars: 25 μm (B); 100 μm (C); 750 μm (E).

changes were detected (not shown). Based on this, the expression pattern and the human disease phenotype of peripheral axon degeneration, we focused our analysis on neuromuscular function and peripheral axons.

Behavioral phenotyping of *Lrsam1* mutant mice

Deficits in neuromuscular performance often result in behavioral abnormalities. Therefore, we assessed coordination using rotarod testing and gait analysis using a treadmill system to determine whether mice lacking *Lrsam1* had motor impairment. Cohorts of 12 (6 males and 6 females) wild-type control, heterozygous and homozygous mice were tested at 6-8 weeks of age. Mice heterozygous or homozygous for the *Lrsam1^{RRK461}* gene trap insertion had the same latency to fall as control mice in the rotarod test. All mice also showed an equivalent improvement in performance in successive trials (Fig. 3A). When walking on a treadmill, *Lrsam1* heterozygotes turned their paws outward and had a wider stance than control mice (Fig. 3B,C; *P*=0.02, one-way ANOVA with Tukey post-hoc test). However, the timing parameters of gait, stride time, stance time and swing time were unchanged, indicating that the mice walked normally (Fig. 3D-F). The treadmill analysis produces many measures of positioning and timing during walking. Stance width and paw angle were chosen for analysis because they are altered in similar analyses in other mouse models of CMT (Cartoni et al., 2010; d'Ydewalle et al., 2011; Filali et al., 2011), and the timing of stance, swing and stride were chosen because they parallel clinical measures in patients. Based on these tests, gross neuromuscular performance is generally unimpaired in *Lrsam1* mutant mice.

Neuromuscular junctions in *Lrsam1* mutant mice

Given the lack of a motor behavioral phenotype in young adult *Lrsam1* mutant mice, we turned to more detailed analyses in older mice, including an examination of neuromuscular junction (NMJ) morphology at 5 months and at >12 months of age to look for signs of die-back neuropathy (Fig. 4). At 5 months, the area of acetylcholine receptor staining and the area circumscribing the NMJs of the tibialis anterior muscle was greater in the heterozygous mutant mice and, similarly, although not significantly, greater in the homozygous mutant mice (Fig. 4A,B). However, the staining intensity of postsynaptic acetylcholine receptors (AChRs) labeled with Alexa- Fluor-594-conjugated α-bungarotoxin (BTX) was not different (Fig. 4C). We also quantified NMJs in which the postsynaptic labeling was no longer a continuous pretzel shape, but was instead disaggregated, a morphology seen in aging mice and in other motor neuron disease and myasthenic syndrome models. Disaggregation was observed in mice lacking *Lrsam1*, but was not significantly increased compared with control muscles (Fig. 4D-F) (Bogdanik and Burgess, 2011; Valdez et al., 2012). Interestingly, the enlarged NMJ phenotype observed at 5 months of age was no longer evident at >12 months of age (Fig. 4G-J). Examples of frank denervation or partial occupancy of the NMJ by the presynaptic motor terminal were not observed at either age. The increases in NMJ area observed in heterozygous mice at 5 months of age (Fig. 4A,B) were significant (*P*<0.05) using a *t*-test for pair-wise comparison of heterozygotes and controls, but not significant if all three genotypes (wild type, heterozygotes and homozygotes) were compared using a one-way ANOVA. This,
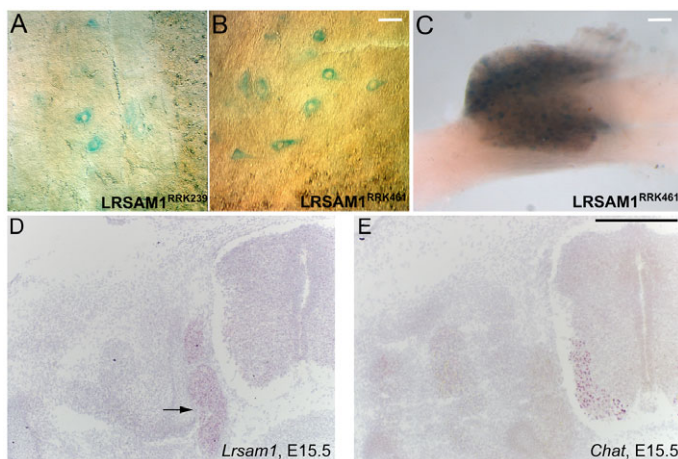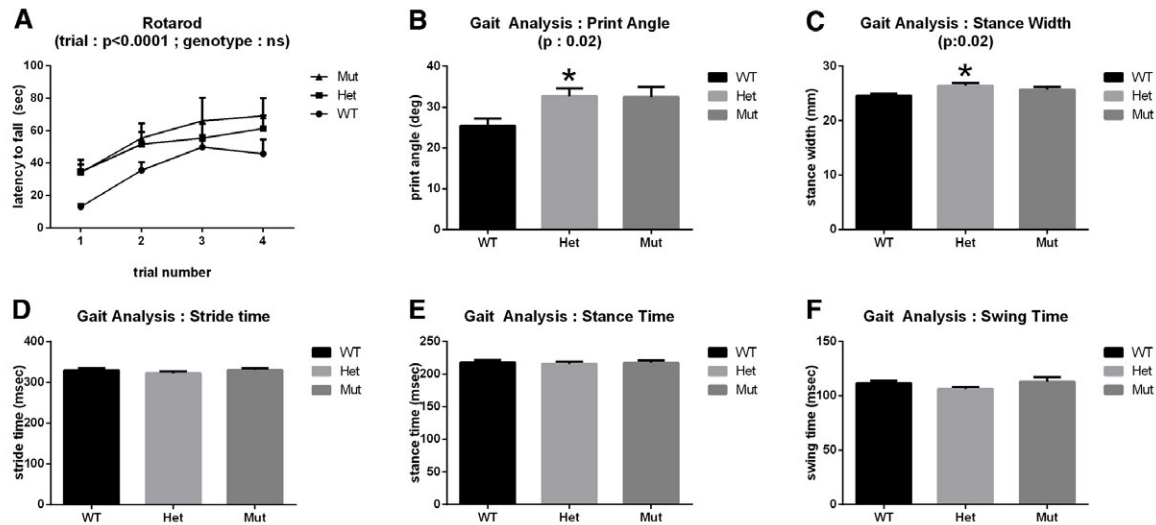
Fig. 3. Neuromuscular performance in *Lrsam1* mutant mice. Wild-type, heterozygous and homozygous mutant mice were tested on a rotarod and in a treadmill analysis of gait. (A) All mice showed an improvement in performance on the rotarod (increased latency to fall) with repeated trials, but no significant effects of genotype were found. (B,C) In an analysis of gait, mice lacking *Lrsam1* were found to hold their paws at a wider angle (B) and to have a wider stance (C). Averages for the left and right hindlimbs are shown. (D-F) The dynamic parameters of gait: stride time (the time from one step to the next), stance time (the duration of contact between the paw and the treadmill) and swing time (the duration the paw is in the air during the step) did not change with the loss of *Lrsam1*. Again, results are shown for the hindlimbs. Each genotype cohort consisted of 12 mice, 6 males and 6 females, tested at 6-8 weeks of age. Statistical significance of the ANOVA is given above the graphs when $P<0.05$; significant differences found by a post-hoc Tukey test between heterozygotes or homozygotes and their wild-type controls are shown by asterisks.

combined with the absence of a difference at 12 months of age, suggests that NMJ morphology is quite normal overall.

Peripheral axons and muscle in *Lrsam1* mutant mice

We next examined peripheral nerves and muscle in mice >12 months of age for signs of neuropathy or neurogenic atrophy in aged mice carrying the *RRK461* insertion. The *Lrsam1* heterozygous and homozygous mutant mice did not differ from controls in body weight or muscle to body weight ratios in four hindlimb muscles (not shown), suggesting that there is no muscle atrophy with reduced *Lrsam1*. Consistent with this, muscle histology did not reveal signs of dystrophy or neurogenic atrophy such as angular fibers, central nuclei or fibrosis in mutant animals in the tibialis anterior muscle, which showed the greatest skewing of muscle weight to body weight ratio of the four muscles analyzed (Fig. 5A).

The femoral nerve consists of a primarily motor branch that innervates the quadriceps and a primarily sensory branch that becomes the saphenous nerve distally and innervates the skin of the lower leg. In *Lrsam1* heterozygous or homozygous mutant mice at >12 months of age, the number of axons in the motor branch of the femoral nerve was slightly reduced compared with wild-type littermate controls in both heterozygous and homozygous mice, although the cross-sectional area of the axons was unchanged (Fig. 5B,C). The sensory branch of the femoral nerve showed a similar trend for axon number. Sensory axon area was more variable and showed a reduction in heterozygous mice and an increase in homozygotes (Fig. 5D,E). In analyzing nerve conduction velocities (NCVs), there were no changes in heterozygous or homozygous *Lrsam1* mutant mice (Fig. 5F). Although this is

anticipated for an axonal neuropathy in humans, other mouse models of axonal neuropathy have reduced conduction velocities, probably resulting from reduced axon diameters (Seburn et al., 2006; Motley et al., 2011). The amplitude of the compound muscle action potentials in the thenar muscles of the hind paw were also not significantly different (Fig. 5G). Overall, the peripheral nervous system of the *Lrsam1* mutant mice was quite normal both anatomically and functionally, with no signs of muscle atrophy or reduced axonal conduction, and only minor variability in sensory axon size and a slight decrement in motor axon number.

Lrsam1 mice are more sensitive to acrylamide

To determine whether the *Lrsam1* mutant axons are indeed compromised, we challenged the mice with acrylamide, a neurotoxic agent that causes axon degeneration. Acrylamide was added to the drinking water of 5-month-old mice for 2 weeks, and the measures of peripheral neuropathy described above were repeated in treated and untreated mice, including wild-type, *Lrsam1* heterozygous and *Lrsam1* homozygous littermates. After 2 weeks of acrylamide treatment, the wild-type, heterozygous and homozygous mutant mice showed overt signs of neurological dysfunction, including tremor and poor coordination. However, quantitative measures demonstrated that the degeneration was more severe in the mutant animals. No changes in NCVs were seen in untreated mice across genotypes; however, following acrylamide treatment NCVs showed a significant decrease in *Lrsam1* homozygous mice compared with untreated values and an intermediate decrease, although not statistically significant, was seen in heterozygous mice (Fig. 6A). Axon counts in the motor branch of the femoral nerve revealed a similar profile, with no
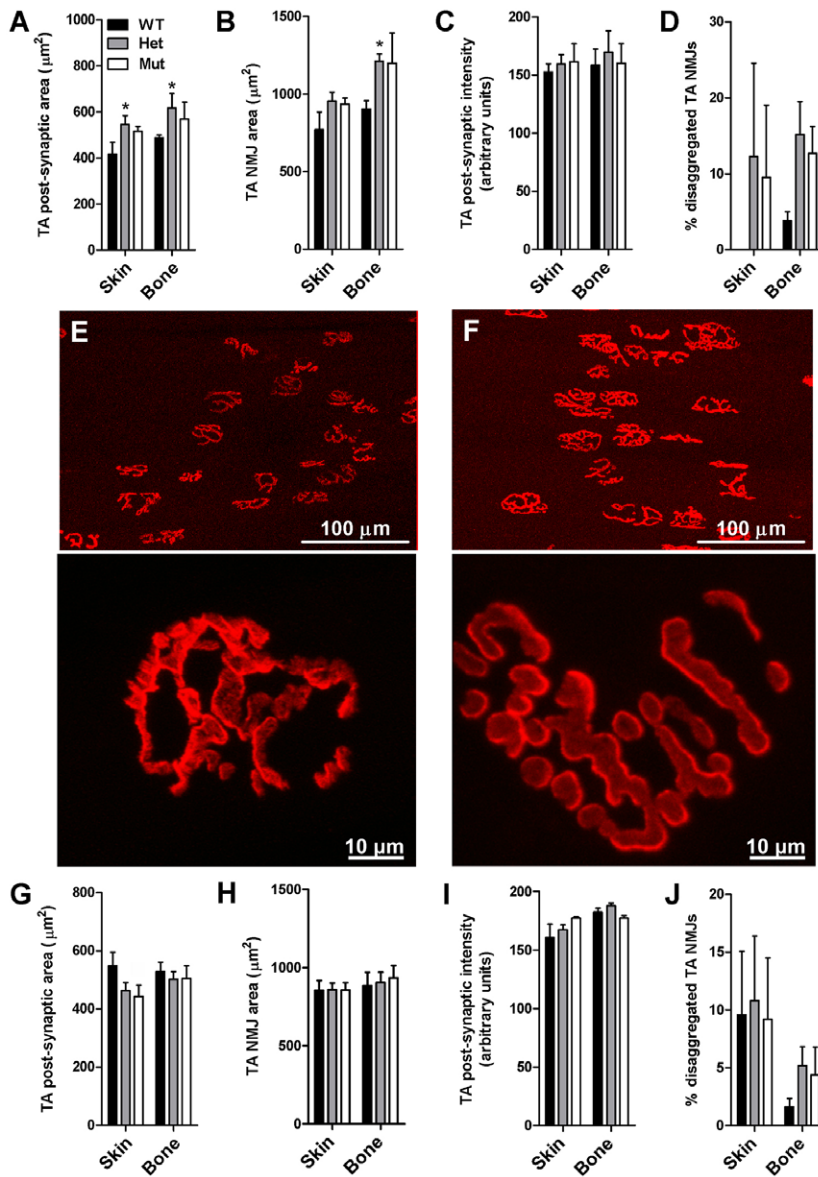
Fig. 4. Neuromuscular junction phenotype in 5- and 12-month-old *Lrsam1^{RRK461}* mice. Neuromuscular junctions (NMJs) were studied from the tibialis anterior muscle of 5-month-old (A-F) and 12-month-old (G-H) mice heterozygous (HET) and homozygous (Mut) for the *Lrsam1^{RRK461}* gene trap allele. The skin-facing and bone-facing regions of the tibialis anterior (TA) muscle have different fiber-type composition and were studied separately. (A,G) The postsynaptic area covered by acetylcholine receptors was significantly increased in 5-month-old heterozygotes (compared with the wild type, *$P<0.05$, *t*-test), but not homozygotes ($P=0.06$ for the skin region and $P=0.16$ for the bone region). This difference was not maintained in 12-month-old mice (G). (B,H) The total NMJ area, defined as the roughly circular surface delimited by the outer-most margins of the NMJ, showed a significant increase in the bone region of the heterozygotes (*$P=0.01$, *t*-test) at 5 months of age, but this was again not detected at 12 months of age (H). (C,I) The intensity of bungarotoxin labeling of the acetylcholine receptors was not altered at either age. (D,J) The percentage of disaggregated NMJs, defined as fragmented or discontinuous bungarotoxin-positive profiles, was also not significantly different at either age. (E,F) Images of representative wild-type (E) and mutant (F) NMJs at 5 months of age. Four mice per genotype were studied in A-D, and 5 in G-J.

changes across genotypes observed without treatment and a reduction in axon numbers in heterozygous mutant mice after treatment (Fig. 6B). Axon cross-sectional areas were not different in any genotype before treatment, but were reduced in homozygous mice after treatment, suggesting a preferential loss of large diameter axons (Fig. 6C). The sensory branch of the femoral nerve was different in that all genotypes showed a decrease in axon number following acrylamide treatment, but there was no significant interaction between the treatment and the genotypes, suggesting that this reduction was not influenced by the *Lrsam1* genotype (Fig. 6D). There were no significant changes in sensory axon cross-sectional areas among genotypes and between treated and untreated animals (Fig. 6E). Thus, sensory axons are sensitive to acrylamide, but the loss of *Lrsam1* does not further sensitize these axons to degeneration, whereas axons of the motor branch of the femoral nerve showed greater sensitivity to acrylamide-induced degeneration when *Lrsam1* levels were reduced. These effects were observed in 5-month-old mice, when no peripheral axon phenotype was otherwise present.

Subcellular localization of LRSAM1

We next examined the plausibility of our hypothesized pathophysiological mechanism relating to late endosome to lysosome sorting and TSG101 association. Unfortunately, the commercial antibody against LRSAM1 that worked for western blotting was inadequate for immunocytochemistry on tissue sections, possibly due to low protein levels *in vivo* and poor specificity as indicated by the western blot. We therefore turned to transfected cells, which we were also able to co-label with markers of various subcellular compartments. The rabbit anti-LRSAM1 antibody worked well in these assays and staining transfected COS7 or CHO cells with this antibody completely overlapped staining with an anti-MYC antibody recognizing the C-terminal epitope tag present on the LRSAM1 cDNA expression
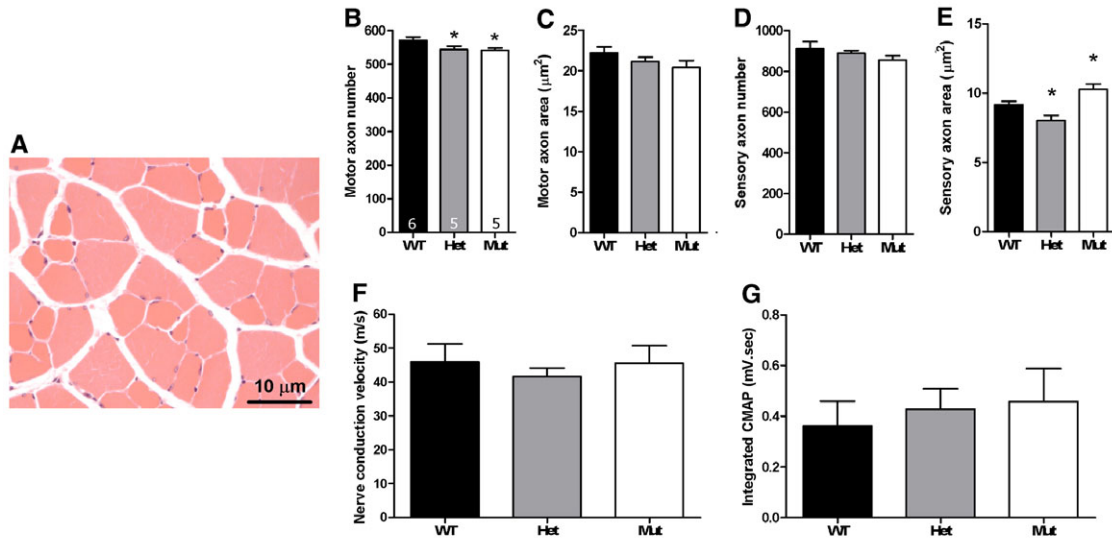
Disease Models & Mechanisms • DMM

Fig. 5. Muscle and nerve phenotypes in 12-month-old _Lrsam1_^RRK461^. (A) Tibialis anterior cross-section from a mutant mouse stained with hematoxylin and eosin did not reveal muscle pathology. (B-E) Analysis of the axons of the motor (B,C) and sensory (D,E) branches of the femoral nerve. Axon counts are shown in B and D; axon cross-sectional areas are shown in C and E. A slight but significant decrease in the motor axon number was found in the heterozygous and homozygous mutants. In sensory axons, heterozygotes displayed a decrease in the average diameter and homozygotes showed an increase in the average diameter, owing to the larger variability in these axons. (F,G) Nerve conduction velocity measured between the sciatic notch and the lumbrical muscle of the foot and the integrated compound muscle axon potential (CMAP) in the lumbrical muscle were not affected in the _Lrsam1_^RRK461^ mice. *$P<0.05$, t-test. Animal numbers: (B-E) 6 wild type, 5 heterozygous and 5 homozygous mutants; (F,G) 7 wild type, 13 heterozygous and 5 homozygous mutants.

construct (Fig. 7A,B). Using transfected COS7 cells, we found minimal overlap with endogenous GM130, a marker of the Golgi complex in all transfected cells (Fig. 7C); however, the bulk of the LRSAM1 labeling was in a perinuclear compartment surrounding the GM130-positive Golgi. Co-labeling with p230, a marker of the trans-Golgi, produced results very similar to GM130 (not shown), so the identity of this structure remains unclear. We were concerned that this localization could be due to overexpression in transfected

cell system. However, using the same techniques and expression vector following transfection with PLA2G6 (phospholipase a2 group 6, or IPLA2β), which is another intracellular, cytoplasmic protein of comparable size (807 amino acids), we did not observe a pattern surrounding GM130 (Fig. 7D). LRSAM1 was also present in cytoplasmic puncta. Therefore, we examined the localization of LRSAM1 in other subcellular compartments, including the early endosome labeled with EEA1 (early endosomal antigen 1) and the
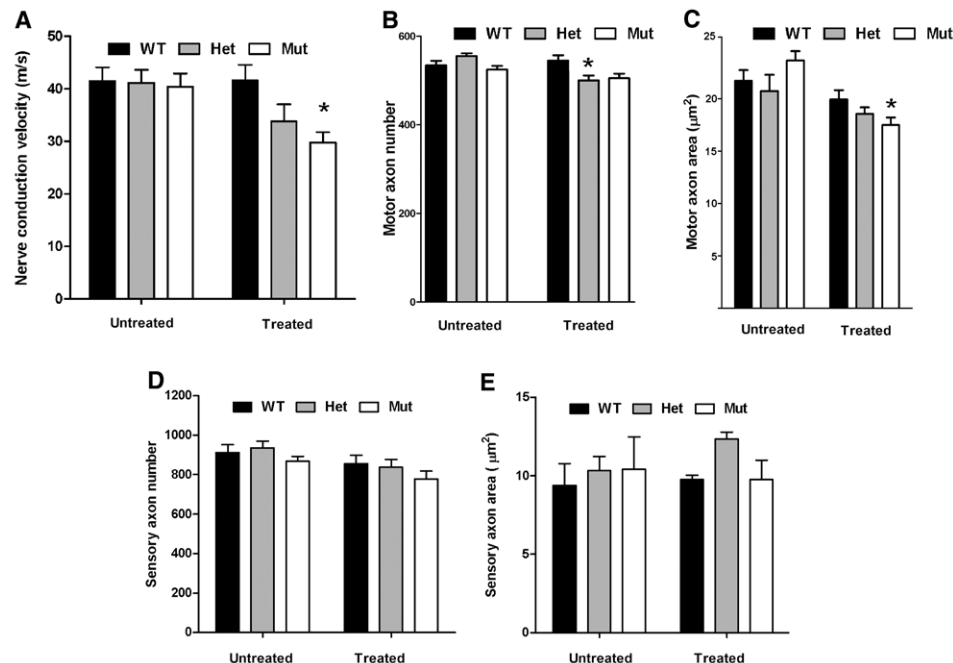

Fig. 6. Acrylamide-induced axon degeneration in 5-month-old _Lrsam1_^RRK461^ mice. (A) Nerve conduction velocity (NCV) measured between the sciatic notch and the lumbrical muscle of the foot did not vary between genotypes without acrylamide treatment. Acrylamide treatment resulted in a significant decrease in the NCV in homozygous mutant mice. (B,C) With acrylamide treatment, motor axons of the femoral nerve were reduced in number in heterozygous mice and cross-sectional area in homozygous mice. For both the axon counts and cross-sectional area, a significant interaction was noted between treatment and genotype (two-way ANOVA, *$P<0.05$). (D,E) Sensory axons of the femoral nerve were reduced in number by the acrylamide treatment regardless of genotype (two-way ANOVA: treatment, $P<0.05$; genotype × treatment interaction, $P>0.05$), but were unchanged in area. Animal numbers: (A-C) 6 wild type, 10 heterozygotes and 10 homozygotes untreated; 6 wild type, 12 heterozygotes and 10 homozygotes treated; (D,E) 6 wild type, 6 heterozygous and 6 homozygous untreated; and 3 wild type, 7 heterozygotes and 7 homozygous treated nerves.
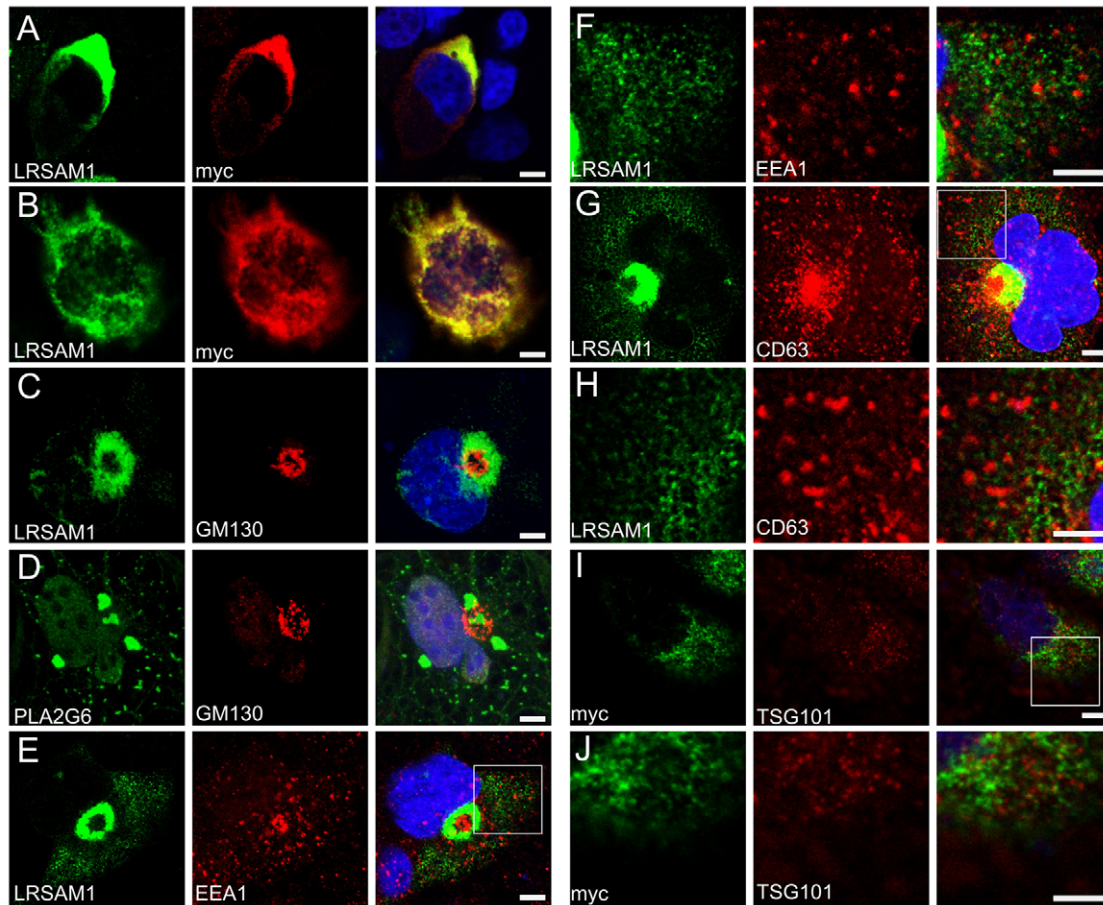
Fig. 7. Subcellular localization of LRSAM1 in transfected cells. COS7 and CHO cells were transfected with an LRSAM1 expression construct that also encodes a C-terminal MYC epitope tag. (A,B) Double labeling of COS7 (A) and CHO (B) cells with anti-LRSAM1 and anti-MYC produced complete overlap with the exception of some anti-LRSAM1-positive puncta in the nuclei of CHO cells. (C) Double labeling with anti-LRSAM1 and GM130, a marker of the Golgi, revealed minimal overlap, with a majority of the LRSAM1 labeling surrounding the GM130 signal. (D) The LRSAM1 pattern was not an artifact of transfection because a control cytoplasmic protein, PLA2G6, expressed by the same vector produced a very different pattern. (E) LRSAM1 showed little overlap with early endosomal antigen 1 (EEA1). (F) A higher magnification view of EEA1 and LRSAM1 in the cytoplasm. (G,H) Outside the Golgi, LRSAM1 also failed to overlap with CD63, a marker of late endosomes. (I,J) In CHO cells, recombinant LRSAM1 labeled with anti-MYC showed nominal overlap with TSG101. Nuclei are counterstained with DAPI. Regions of higher magnification in F, H and J are noted by frames in E, G and I. Scale bars: 10 μm.

late endosome labeled with CD63, and found no overlap with LRSAM1 labeling outside of the Golgi (Fig. 7E-H). We also examined localization with TSG101 and found no appreciable overlap (Fig. 7I,J). The TSG101 experiments were performed in CHO (Chinese hamster ovary) cells because we could not get convincing TSG101 labeling in COS7 cells. To avoid the nonspecific nuclear labeling sometimes observed in CHO cells with the anti-LRSAM1 antibody, we used anti-MYC to specifically recognize the epitope tag on the recombinant LRSAM1. In fact, all experiments above were performed in CHO cells in addition to the COS7 cells shown, with similar results. Therefore, in transfected cells, LRSAM1 is primarily found in a perinuclear compartment surrounding the Golgi and does not colocalize in the cytoplasm with early or late endosomal markers nor with TSG101.

DISCUSSION
In this study we have shown that a loss-of-function mutation in the mouse *Lrsam1* gene sensitizes peripheral motor axons to

acrylamide-induced degeneration. Modest differences in the area of NMJs in young mice, and in axon number in the periphery in old mice, were also observed, but the phenotype is very mild in the absence of a neuronal challenge.

Mutations in human *LRSAM1* cause an axonal neuropathy, designated CMT2P (OMIM614436), that is also mild (Guernsey et al., 2010; Weterman et al., 2012; Nicolaou et al., 2012). Patients are typically diagnosed in their 20s or 30s. Muscle wasting in the hands and especially feet is observed, as well as a lack of tendon reflexes and variable sensory involvement, primarily affecting vibration sense, but also proprioception and pain. Electrophysiological studies are consistent with axonal neuropathy, with no reduction in NCVs; sural nerve biopsy of one patient showed axonal degeneration. Autonomic symptoms were not consistently reported.

Three families have been identified with *LRSAM1*-associated neuropathy, one with recessive and two with dominant inheritance. The recessive mutation found in a Canadian pedigree is a frame

shift creating a premature stop codon at position 643 of 723 (Guernsey et al., 2010). This allele results in a loss-of-function mutation that produces no detectable (by western blotting) protein. In contrast, the dominant mutation identified in a Dutch pedigree is a frameshift mutation in the final exon. This allele (L708Rfx28) changes the last 16 amino acids and extends the reading frame by an additional 12 residues before a stop codon is reached (Weterman et al., 2012). This mutation, and the mutation found in the Sardinian pedigree (A683Pfx3) (Nicolaou et al., 2012), are predicted to affect the C-terminal ring domain (aa 675-710) required for ubiquitin transfer and ligase activity. However, because the mutations are in the terminal exon and are unlikely to result in nonsense-mediated decay of the mRNA, and because patients are comparable in severity to the Canadian-null patients, it is also possible that the mutant protein causes a dominant negative effect. Consistent with this, a truncated LRSAM1 protein product was indeed detected in a patient with the A683Pfx3 allele. Therefore, we suggest a dominant negative mechanism in the Dutch and Sardinian families, in which the altered sequence at the C-terminus could interfere with the function of wild-type proteins. Furthermore, we saw that LRSAM1 protein was potentially in multimers on western blots from transfected cells, suggesting that the mutant protein is directly interacting with and inhibiting the wild-type protein (Fig. 1B). However, we were not able to detect these higher molecular weight species in mouse tissue lysates, even under non-reducing conditions (not shown), so their existence *in vivo* remains speculative. Furthermore, we did note intermediate phenotypes in heterozygous mice, suggesting some degree of haploinsufficiency, but these phenotypes were milder than in homozygotes. The greater than 50% reduction in *Lrsam1* transcript in heterozygotes might indicate some autoregulatory feedback mechanism and also suggests that the dosage dependence of the severity of the *Lrsam1* phenotype is not a simple linear relationship with LRSAM1 levels, although protein levels in heterozygous mice were modestly reduced, as anticipated.

The mouse phenotype is quite mild, even with age, but is not a poor model of the relatively mild human disease. The use of challenges such as acrylamide to bring out subclinical phenotypes in mice has been reported previously (Nguyen et al., 2009; Ewaleifoh et al., 2012). This increased sensitivity to chemical agents seen in the mouse model also parallels CMT, where patients show an increased sensitivity to agents such as chemotherapy drugs, which cause axonopathy. Furthermore, mouse models of axonal neuropathy have been problematic in their face validity as human disease models. Many are milder or of later onset than anticipated, for example *Nefl*, whereas others have developmental rather than degenerative phenotypes, such as *Mfn2* (Zhu et al., 1997; Robertson et al., 2002; Detmer et al., 2008). The reason for these discrepancies is not clear, nor is a single explanation likely; however, these models do retain their usefulness for studies to understand the cell biology, biochemistry and genetic interactions of these disease genes in a mammalian system.

The phenotypes of *Lrsam1* mutant mice were most pronounced in motor axons, with the involvement of sensory axons not differing from controls. Phenotypes at the NMJ could be due to *Lrsam1* expression in the motor neurons or in the muscle. We have found *Lrsam1* expression in muscle by RT-PCR (not shown) and at a low level in embryonic muscle by *in situ* hybridization (Fig. 2). The

transcript is enriched in the endplate band of muscle compared with extrasynaptic regions, as shown by microarray expression analysis of microdissected samples (Kishi et al., 2005). Our analysis of expression using the *lacZ* reporter in the gene trap vector in adult mice indicated high expression in motor neurons with little detectable expression in other tissues and cell types, but this analysis might simply be detecting the highest expressing cells. *In situ* hybridization studies in human embryonic tissue also indicated widespread expression, and studies using transgenic mouse models of Huntington's disease have detected *Lrsam1* expression in brain regions (Tang et al., 2011; Weterman et al., 2012).

The subcellular localization of LRSAM1 protein suggests other possible functions besides endosome to lysosome trafficking, although this mechanism is still very attractive and certainly not eliminated by our results. LRSAM1 was placed in this pathway largely due to its association with TSG101, the best characterized substrate of LRSAM1 E3 ubiquitin ligase activity (Amit et al., 2004). TSG101 is involved in the formation of multivesicular bodies, which transit from the late endosome to the lysosome. TSG101 also associates with SIMPLE, a protein that also causes a CMT when mutated (Shirk et al., 2005). Thus, the interaction of LRSAM1 with TSG101 is both attractive and compelling. We, and others, have found that LRSAM1 overexpression can decrease TSG101 levels, consistent with LRSAM1-mediated ubiquitylation causing TSG101 degradation (not shown) (McDonald and Martin-Serrano, 2008). We failed to find appreciable colocalization of transfected LRSAM1 and TSG101 in CHO cells. This is in contrast to a previous study that found colocalization of LRSAM1 with TSG101 immediately below the plasma membrane, using tagged constructs transfected in HELA cells (Amit et al., 2004). However, other studies examining TSG101 (independent of LRSAM1) have not reported this submembrane localization (Xie et al., 1998; Zhong et al., 1998), so it might be cell-type specific, dependent on the stage of the cell cycle, dependent on coexpression with LRSAM1 or an effect of the epitope tag or other experimental conditions. It is also noteworthy that TSG101 is a component of the ESCRT1 complex. ESCRT complexes (of which there are five) are involved in vesicle and membrane scission in many processes, including viral budding and cytokinesis, in addition to multivesicular body formation (Hanson et al., 2009; Raiborg and Stenmark, 2009). Therefore, even if the interaction between LRSAM1 and TSG101 is directly related to CMT, pathways besides late endosome to lysosome trafficking via multivesicular bodies should be considered. Also consistent with alternative functions, LRSAM1 was recently reported to bind bacteria within cells via its leucine-rich repeats and then mediate ubiquitylation of bacterial proteins via its E3 ring domain, thus targeting them for autophagy (Huett et al., 2012). Therefore, the array of substrates and cellular functions of LRSAM1 remain incompletely understood.

Interestingly, SIMPLE shares many functions with LRSAM1. SIMPLE is also proposed to be an E3 ubiquitin ligase and also binds to TSG101, regulating its levels (Saifi et al., 2005; Shirk et al., 2005). Like LRSAM1 in our experiments, SIMPLE also fails to colocalize with TSG101 in transfected HEK293T cells (Shirk et al., 2005). Thus, there are similarities to be drawn at the cellular and molecular level, but the associated diseases are quite different, with LRSAM1 mutations causing axonal neuropathy and SIMPLE mutations causing demyelinating neuropathy. Whether these different

phenotypes are the result of a common function in different cell types caused by different expression patterns or whether this reflects different functions of the two proteins remains to be determined.

We did not find striking colocalization of LRSAM1 with GM130, a marker of the Golgi complex, nor with EEA1 or CD63, which are markers of early and late endosomes, respectively, nor with TSG101. We were concerned that overexpression in transfected cells could lead to the localization surrounding the Golgi, but we did not see an equivalent localization with another cytoplasmic protein, PLA2G6 (IPLA2β), in the same expression vector under equivalent conditions. If the role of LRSAM1 is to regulate TSG101 levels, this could be through interactions during synthesis and trafficking, and not at sites of TSG101 activity such as MVBs. Alternatively, LRSAM1 might be serving other functions and have substrates other than TSG101. Consistent with this, LRSAM1 (RIFLE) has been shown to modulate cell-cell and cell-matrix adhesion and to interact with GSKβ signaling pathways (Li et al., 2003). The identity of the perinuclear compartment surrounding the Golgi that contains the bulk of the LRSAM1 labeling remains unclear.

Our data demonstrate that mice lacking *Lrsam1* have compromised peripheral axons and therefore provide a reasonable model for human CMT2P. Understanding the disease mechanism and the relationship between LRSAM1 and axon integrity will require additional work. Although a pathophysiological mechanism involving endosome to lysosome sorting might be involved, other cellular pathways should also be considered on the basis of the subcellular localization of the protein.

MATERIALS AND METHODS

Mice
All mouse husbandry and procedures were conducted according to the NIH Guide for Care and Use of Laboratory Animals and were approved by The Jackson Laboratory Animal Care and Use Committee. Mice were housed in PIV racks and provided food and water ad libitum. Specific procedures are described below.

Gene trap insertions and genotyping
Gene trap insertions in the mouse *Lrsam1* gene were identified using the Ensemble genome browser and the Mouse Genome Informatics websites (http://www.ensembl.org/index.html and http://www.informatics.jax.org/). ES cell lines with insertions in the *Lrsam1* gene generated by Bay Genomics were ordered from the Mouse Mutant Regional Resource Center (MMRRC). The cell lines were confirmed by PCR and the precise insertion sites were determined by sequencing reaction products produced by amplification from forward primers in exon 21 or 22 of *Lrsam1* (5′-AAGAGGAACTCCATGGCATC-3′ and 5′-GCCTTTGT-CCTTGAAACTGC-3′, respectively) to a reverse primer in the gene trap insertion (5′-GACAGTATCGGCCTCAGGAAGATCG-3′). The RRK239 insertion was determined to be at position 185 of intron 21 and the RRK461 insertion was determined to be at position 1149 of intron 22. Mice were subsequently genotyped using the following primer combinations: LRSAM1[RRK239] common forward: 5′-AACGCTTGTCCCATTGTAGC-3′ and wild-type reverse: 5′-CTGTCCTGGAGAGCCCAGT-3′ or gene-trap reverse: 5′-CTGTCCTCCAGTCTCCTCCA-3′; and LRSAM1[RRK461] common forward: 5′-ATAGGACAGGAGCCACGATG-3′ and

wild-type reverse: 5′-GGACTGGACGTGGGTTTATC-3′ or gene-trap reverse: 5′-CAACCTCCGCAAACTCCTAT-3′. Following validation of the insertions, mice were generated from the ES cell lines by standard blastocyst injection techniques into C57BL/6J hosts. Germline transmission of the insertions by chimeric mice was confirmed by PCR using the primers listed above.

In situ hybridization
In situ hybridization was carried out using the Affymetrix QuantiGene View system, performed by the manufacturer. Briefly, transverse thoracic sections of fresh frozen E15.5 mouse embryos were provided. Sections were post-fixed and treated with protease to improve probe access. Target-specific probe sets were then hybridized to the mRNA in sections and signals amplified through sequential hybridizations, ending with an alkaline phosphatase-conjugated probe that is visualized with Fast-Red substrates.

Rotarod and gait behavioral analyses
Six male and six female mice, all aged 6-8 weeks, of the different genotypes (wild-type, heterozygote and homozygote mutants for the *Lrsam1*[RRK461] gene-trap) were tested on the Rotarod and then on the Treadscan gait analysis system 1 day later. Tests were performed in the morning.

For the rotarod, up to four mice at a time were placed on the stationary rod (Economex Accelerating Rota-Rod – Columbus Instruments, Columbus, OH). When all mice were facing the back of the device, a constant speed of 4.0 rotations/minute with an acceleration of 0.1 rpm/second was applied over a 5-minute period, for four consecutive trials. Latency to fall and behavior was recorded for each trial. Mice were acclimated to the rotarod for a first trial before being scored for the four trials shown on Fig. 3A. A 10-minute (minimum) rest period was allowed between two successive trials.

For the Treadscan analysis, mouse gait was analyzed using a treadmill system with automated analysis of footfalls, as previously described (Wooley et al., 2005; Wooley et al., 2009; Burgess et al., 2010). Briefly, mice were placed on the stationary treadmill (BCamCapture 2.0; CleverSys Inc., Reston, VA) and once the mouse was facing the head of the treadmill, a constant speed of 10 rotations/minute (equal to 167.2 mm/second) was applied. The gait was recorded by a camera located below the treadmill for ~8 seconds. Video recordings were analyzed with the Cleversys TreadScan 4.0 software. Analysis was performed on a minimum of six complete strides taken from a selection of segments from the video where the mouse was running at the speed of the treadmill and was not refusing to walk, rearing or touching the wall of the device.

Western blotting
Spinal cords were homogenized in lysis buffer (150 mM NaCl, 10 mM NaHPO$_4$, 2 mM EDTA, 0.1% SDS, 1% Triton X-100, protease inhibitors). The lysate was cleared by centrifugation at 15,000 *g* for 20 minutes and then 50 μg of protein loaded on a 4-15% acrylamide gradient gel (Mini-PROTEAN® TGX™ Precast Gel, Biorad). Acrylamide gels were run at 200 V for 30 minutes and transferred for 1 hour at 100 V on PVDF membranes. The membranes were subsequently blocked in 2% milk in TBS-0.1% Tween20 and incubated overnight at 4°C with the primary antibody

(mouse anti-LRSAM1, Abcam ab73113; rabbit anti-LRSAM1, Sigma-Aldrich HPA021403; rabbit anti-GAPDH, Abcam ab9385; or mouse anti-tubulin, clone DM1A, Sigma-Aldrich T9026) diluted in the blocking solution. Horseradish peroxidase (HRP)-conjugated secondary antibodies were applied for 2 hours at room temperature in the blocking solution and the membranes visualized by reaction with the Western Lightning Chemiluminescence Reagent (Perkin Elmer). BioMax MS Films (Kodak) were used for maximum detection. Protein domain predictions were made using ELM software (Dinkel et al., 2012).

Quantitative RT-PCR

Spinal cord RNAs were extracted with the TRIzol protocol (Invitrogen, 15596-026) and assessed for purity on a Nanodrop spectrophotometer (ThermoScientific). Only samples with a 260/280 nm ratio above 1.9 were used. Then, 500 ng of total RNAs were reverse-transcribed with oligo dT following the manufacturer's instructions (SuperScript™ III Reverse Transcriptase, Invitrogen, 18080-093) and 50 or 10 ng of cDNA were used per qRT-PCR reaction. qRT-PCR reactions were run with the SYBR-Green PCR master mix (Applied Biosystems) on a 7500 Real-Time PCR System (Applied Biosystems). Primer pairs were designed in 5′ (Exon 8 forward: 5′-AGAAATCAACTCACGC-ATCTCC-3′ and Exon 9 reverse: 5′-CCAGGGTGTCAGGA-AGCTC-3′) and 3′ (Exon 25 forward: 5′-CTCGAGAATGAG-GTCCTTGG-3′ and Exon 26 reverse: 5′-GCTGACAGCAGC-AGACGTG-3′) of *Lrsam1* cDNA to study the variations in transcript abundance upstream and downstream of the gene trap insertion sites. GAPDH (PrimerBank ID 6679937a1, 5′-AGGTCGGTGTGAACGGATTTG-3′ and 5′-TGTAGACCATGT-AGTTGAGGTCA-3′) was used as the reference gene. We verified that all primers presented the same amplification efficiency for a range of 1 to 100 ng cDNA per PCR reaction and used the ΔΔCt method to represent the fold-change of each target mRNA in the mutant samples compared with the wild-type one. Error bars represent the extreme values of the fold change, incorporating the standard deviations of the mutant ΔCts.

NMJ staining and quantification

Neuromuscular junction imaging was performed as described (Burgess et al., 2010; Bogdanik and Burgess, 2011). In brief, muscles were dissected and fixed in cold 2% buffered paraformaldehyde (prepared fresh) overnight. Muscles were embedded in 3% agarose in PBS and sectioned (100-μm thick sections) with a vibratome. Sections were then incubated overnight in primary antibody (a cocktail of mouse monoclonal anti-neurofilament 2H3 and anti-SV2 from the Developmental Studies Hybridoma Bank), washed the following day and incubated overnight with Alexa-Fluor-488 conjugated anti-mouse IgG1 and Alexa-Fluor-594 conjugated α-bungarotoxin (BTX, Invitrogen). Muscles were mounted in fluorescence mounting medium (DAKO, S3023) and imaged on a Leica SP5 laser confocal microscope.

For semi-quantitative imaging, control and mutant tissues were processed for immunofluorescence in parallel and images were acquired by confocal microscopy with the equivalent settings (laser power, gain, magnification and thickness of the stacks). Image analysis was performed with ImageJ. For NMJ morphometry, images were collected with a 20× objective. To measure the post-synaptic area, acetylcholine receptor clusters were thresholded and their area and intensity measured. To measure the NMJ area, the outer perimeter delimiting each NMJ was drawn by hand and the surface enclosed measured. Between 20 and 40 NMJs per mouse were analyzed, on at least three mice per genotype and age group. Areas in pixels were converted into square microns based on the confocal settings and mean intensities in the BTX channel (8-bits) and expressed as arbitrary units.

Nerve conduction velocities

Sciatic nerve conduction velocity was determined by measuring the latency of compound motor action potentials recorded in the muscle of the left rear paw. Mice were anesthetized with 1.5-2.0% isofluorane and placed on a thermostatically regulated heating pad to maintain normal body temperature. Action potentials were evoked by subcutaneous stimulation at the sciatic notch and at the ankle. The distance between points of stimulation combined with the latencies was used in the calculation of velocity. For recording, the active needle electrode was inserted in the center of the paw and a reference electrode was placed in the skin between the first and second digits.

Nerve histology and quantification

The sensory and motor branches of the femoral nerve were isolated and fixed overnight in 2% glutaraldehyde and 2% paraformaldehyde in 0.1 M cacodylate buffer. The tissue was then processed for transmission electron microscopy (TEM) and embedded in plastic before 0.5-μm sections were cut and stained with toluidine blue. For more information see published description (Burgess et al., 2010). For axon counting and axon diameter measurement, images were captured using a Nikon Eclipse E600 microscope with a 40× objective. An automated count of the axons and measurement of their cross-sectional area was performed with ImageJ. Nerve section pictures were converted to 8-bit pictures and the threshold function was used to highlight the axoplasm of as many axons as possible. The resulting binary picture was analyzed with the Analyze Particles plug-in to count and measure the area of every particle with an area above 30 pixels (the area of the smallest axons) and with a circularity above 0.5 (to eliminate the thresholded regions between the axons). Axons that were not captured by the plug-in were afterwards selected manually, counted and the area of their axoplasm, selected with the Wand tool, measured.

Acrylamide treatment

Mice were treated with acrylamide added to the drinking water at 400 ppm for 2 weeks according to published methods (Nguyen et al., 2009), and then immediately taken for analysis.

Statistical analysis

When comparing values from heterozygous or homozygous mutant mice with values from control littermates (Fig. 4), a Student's *t*-test was used. When the effects of two factors (genotype and trial number, Fig. 3A, and genotype and acrylamide treatment, Fig. 6) were analyzed, a two-way ANOVA followed by a post-hoc Bonferroni test was used. When the effect of the genotype was analyzed in the locomotion tests (Fig. 3B-E), a one-way ANOVA followed by a post-hoc Tukey test was used. Thresholds of $P<0.05$ were considered significant.

Cell transfection and labeling

COS7 and CHO cells were grown in DMEM medium (Invitrogen) with 10% FBS (Atlanta Biologicals) in the absence of antibiotics at 37°C with 5% CO_2. cDNA expression constructs encoding LRSAM1 or PLA2G6 in the APtag-5 vector (Gene Hunter) with a MYC tag at the C-terminus were generated and transfected into cells using Lipofectamine 2000. After 24 hours, the media was removed and cells rinsed and fixed with 4% buffered paraformaldehyde for 10 minutes. Cells were then labeled for immunofluorescence using the following primary antibodies at a 0.5 µg/m final concentration: anti-LRSAM1 (rabbit; Sigma, #HPA021403), anti-GM130 (mouse; Covance, #MMS-147P-100), anti-EEA1 (mouse; BD Transduction Laboratories, #610456), anti-CD63, anti-TSG101 (mouse and goat; Santa Cruz Biotechnology, #5275 and #6037), anti-MYC (mouse, clone 9E10; Developmental Studies Hybridoma Bank) and the following fluorescently conjugated secondary antibodies: Alexa Fluor® 488 donkey anti-rabbit IgG, Alexa Fluor® 594 donkey anti-mouse IgG and Alexa Fluor® 594 donkey anti-goat IgG (Invitrogen).

REFERENCES
Amit, I., Yakir, L., Katz, M., Zwang, Y., Marmor, M. D., Citri, A., Shtiegman, K., Alroy, I., Tuvia, S., Reiss, Y. et al. (2004). Tal, a Tsg101-specific E3 ubiquitin ligase, regulates receptor endocytosis and retrovirus budding. *Genes Dev.* **18**, 1737-1752.

Bogdanik, L. P. and Burgess, R. W. (2011). A valid mouse model of AGRIN-associated congenital myasthenic syndrome. *Hum. Mol. Genet.* **20**, 4617-4633.

Burgess, R. W., Skarnes, W. C. and Sanes, J. R. (2000). Agrin isoforms with distinct amino termini: differential expression, localization, and function. *J. Cell Biol.* **151**, 41-52.

Burgess, R. W., Cox, G. A. and Seburn, K. L. (2010). Neuromuscular disease models and analysis. *Methods Mol. Biol.* **602**, 347-393.

Cartoni, R., Arnaud, E., Medard, J. J., Poirot, O., Courvoisier, D. S., Chrast, R. and Martinou, J. C. (2010). Expression of mitofusin 2(R94Q) in a transgenic mouse leads to Charcot-Marie-Tooth neuropathy type 2A. *Brain* **133**, 1460-1469.

Chow, C. Y., Zhang, Y., Dowling, J. J., Jin, N., Adamska, M., Shiga, K., Szigeti, K., Shy, M. E., Li, J., Zhang, X. et al. (2007). Mutation of FIG4 causes neurodegeneration in the pale tremor mouse and patients with CMT4J. *Nature* **448**, 68-72.

Chow, C. Y., Landers, J. E., Bergren, S. K., Sapp, P. C., Grant, A. E., Jones, J. M., Everett, L., Lenk, G. M., McKenna-Yasek, D. M., Weisman, L. S. et al. (2009). Deleterious variants of FIG4, a phosphoinositide phosphatase, in patients with ALS. *Am. J. Hum. Genet.* **84**, 85-88.

d'Ydewalle, C., Krishnan, J., Chiheb, D. M., Van Damme, P., Irobi, J., Kozikowski, A. P., Vanden Berghe, P., Timmerman, V., Robberecht, W. and Van Den Bosch, L. (2011). HDAC6 inhibitors reverse axonal loss in a mouse model of mutant HSPB1-induced Charcot-Marie-Tooth disease. *Nat. Med.* **17**, 968-974.

Detmer, S. A., Vande Velde, C., Cleveland, D. W. and Chan, D. C. (2008). Hindlimb gait defects due to motor axon loss and reduced distal muscles in a transgenic mouse model of Charcot-Marie-Tooth type 2A. *Hum. Mol. Genet.* **17**, 367-375.

Dinkel, H., Michael, S., Weatheritt, R. J., Davey, N. E., Van Roey, K., Altenberg, B., Toedt, G., Uyar, B., Seiler, M., Budd, A. et al. (2012). ELM – the database of eukaryotic linear motifs. *Nucleic Acids Res.* **40**, D242-D251.

Ewaleifoh, O., Trinh, M., Griffin, J. W. and Nguyen, T. (2012). A novel system to accelerate the progression of nerve degeneration in transgenic mouse models of neuropathies. *Exp. Neurol.* **237**, 153-159.

Filali, M., Dequen, F., Lalonde, R. and Julien, J. P. (2011). Sensorimotor and cognitive function of a NEFL(P22S) mutant model of Charcot-Marie-Tooth disease type 2E. *Behav. Brain Res.* **219**, 175-180.

Fuerst, P. G., Bruce, F., Tian, M., Wei, W., Elstrott, J., Feller, M. B., Erskine, L., Singer, J. H. and Burgess, R. W. (2009). DSCAM and DSCAML1 function in self-avoidance in multiple cell types in the developing mouse retina. *Neuron* **64**, 484-497.

Guernsey, D. L., Jiang, H., Bedard, K., Evans, S. C., Ferguson, M., Matsuoka, M., Macgillivray, C., Nightingale, M., Perry, S., Rideout, A. L. et al. (2010). Mutation in the gene encoding ubiquitin ligase LRSAM1 in patients with Charcot-Marie-Tooth disease. *PLoS Genet.* **6**, e1001081.

Hanson, P. I., Shim, S. and Merrill, S. A. (2009). Cell biology of the ESCRT machinery. *Curr. Opin. Cell Biol.* **21**, 568-574.

Huett, A., Heath, R. J., Begun, J., Sassi, S. O., Baxt, L. A., Vyas, J. M., Goldberg, M. B. and Xavier, R. J. (2012). The LRR and RING domain protein LRSAM1 is an E3 ligase crucial for ubiquitin-dependent autophagy of intracellular Salmonella Typhimurium. *Cell Host Microbe* **12**, 778-790.

Kishi, M., Kummer, T. T., Eglen, S. J. and Sanes, J. R. (2005). LL5beta: a regulator of postsynaptic differentiation identified in a screen for synaptically enriched transcripts at the neuromuscular junction. *J. Cell Biol.* **169**, 355-366.

Lee, S. M., Olzmann, J. A., Chin, L. S. and Li, L. (2011). Mutations associated with Charcot-Marie-Tooth disease cause SIMPLE protein mislocalization and degradation by the proteasome and aggresome-autophagy pathways. *J. Cell Sci.* **124**, 3319-3331.

Li, B., Su, Y., Ryder, J., Yan, L., Na, S. and Ni, B. (2003). RIFLE: a novel ring zinc finger-leucine-rich repeat containing protein, regulates select cell adhesion molecules in PC12 cells. *J. Cell. Biochem.* **90**, 1224-1241.

McDonald, B. and Martin-Serrano, J. (2008). Regulation of Tsg101 expression by the steadiness box: a role of Tsg101-associated ligase. *Mol. Biol. Cell* **19**, 754-763.

Moriwaki, Y., Begum, N. A., Kobayashi, M., Matsumoto, M., Toyoshima, K. and Seya, T. (2001). Mycobacterium bovis Bacillus Calmette-Guerin and its cell wall complex induce a novel lysosomal membrane protein, SIMPLE, that bridges the missing link between lipopolysaccharide and p53-inducible gene, LITAF(PIG7), and estrogen-inducible gene, EET-1. *J. Biol. Chem.* **276**, 23065-23076.

Motley, W. W., Seburn, K. L., Nawaz, M. H., Miers, K. E., Cheng, J., Antonellis, A., Green, E. D., Talbot, K., Yang, X. L., Fischbeck, K. H. et al. (2011). Charcot-Marie-Tooth-linked mutant GARS is toxic to peripheral neurons independent of wild-type GARS levels. *PLoS Genet.* **7**, e1002399.

Nguyen, T., Mehta, N. R., Conant, K., Kim, K. J., Jones, M., Calabresi, P. A., Melli, G., Hoke, A., Schnaar, R. L., Ming, G. L. et al. (2009). Axonal protective effects of the myelin-associated glycoprotein. *J. Neurosci.* **29**, 630-637.

Nicolaou, P., Cianchetti, C., Minaidou, A., Marrosu, G., Zamba-Papanicolaou, E., Middleton, L. and Christodoulou, K. (2012). A novel LRSAM1 mutation is associated with autosomal dominant axonal Charcot-Marie-Tooth disease. *Eur. J. Hum. Genet.* **21**, 190-194.

Raiborg, C. and Stenmark, H. (2009). The ESCRT machinery in endosomal sorting of ubiquitylated membrane proteins. *Nature* **458**, 445-452.

Roberts, R. C., Peden, A. A., Buss, F., Bright, N. A., Latouche, M., Reilly, M. M., Kendrick-Jones, J. and Luzio, J. P. (2010). Mistargeting of SH3TC2 away from the recycling endosome causes Charcot-Marie-Tooth disease type 4C. *Hum. Mol. Genet.* **19**, 1009-1018.

Robertson, J., Kriz, J., Nguyen, M. D. and Julien, J. P. (2002). Pathways to motor neuron degeneration in transgenic mouse models. *Biochimie* **84**, 1151-1160.

Saifi, G. M., Szigeti, K., Wiszniewski, W., Shy, M. E., Krajewski, K., Hausmanowa-Petrusewicz, I., Kochanski, A., Reeser, S., Mancias, P., Butler, I. et al. (2005). SIMPLE mutations in Charcot-Marie-Tooth disease and the potential role of its protein product in protein degradation. *Hum. Mutat.* **25**, 372-383.

Seburn, K. L., Nangle, L. A., Cox, G. A., Schimmel, P. and Burgess, R. W. (2006). An active dominant mutation of glycyl-tRNA synthetase causes neuropathy in a Charcot-Marie-Tooth 2D mouse model. *Neuron* **51**, 715-726.

Senderek, J., Bergmann, C., Stendel, C., Kirfel, J., Verpoorten, N., De Jonghe, P., Timmerman, V., Chrast, R., Verheijen, M. H., Lemke, G. et al. (2003). Mutations in a gene encoding a novel SH3/TPR domain protein cause autosomal recessive Charcot-Marie-Tooth type 4C neuropathy. *Am. J. Hum. Genet.* **73**, 1106-1119.

Shirk, A. J., Anderson, S. K., Hashemi, S. H., Chance, P. F. and Bennett, C. L. (2005). SIMPLE interacts with NEDD4 and TSG101: evidence for a role in lysosomal sorting and implications for Charcot-Marie-Tooth disease. *J. Neurosci. Res.* **82**, 43-50.

Stendel, C., Roos, A., Kleine, H., Arnaud, E., Ozçelik, M., Sidiropoulos, P. N., Zenker, J., Schüpfer, F., Lehmann, U., Sobota, R. M. et al. (2010). SH3TC2, a protein mutant

in Charcot-Marie-Tooth neuropathy, links peripheral nerve myelination to endosomal recycling. *Brain* **133**, 2462-2474.

Street, V. A., Bennett, C. L., Goldy, J. D., Shirk, A. J., Kleopa, K. A., Tempel, B. L., Lipe, H. P., Scherer, S. S., Bird, T. D. and Chance, P. F. (2003). Mutation of a putative protein degradation gene LITAF/SIMPLE in Charcot-Marie-Tooth disease 1C. *Neurology* **60**, 22-26.

Tang, B., Seredenina, T., Coppola, G., Kuhn, A., Geschwind, D. H., Luthi-Carter, R. and Thomas, E. A. (2011). Gene expression profiling of R6/2 transgenic mice with different CAG repeat lengths reveals genes associated with disease onset and progression in Huntington's disease. *Neurobiol. Dis.* **42**, 459-467.

Valdez, G., Tapia, J. C., Lichtman, J. W., Fox, M. A. and Sanes, J. R. (2012). Shared resistance to aging and ALS in neuromuscular junctions of specific muscles. *PLoS ONE* **7**, e34640.

Verhoeven, K., De Jonghe, P., Coen, K., Verpoorten, N., Auer-Grumbach, M., Kwon, J. M., FitzPatrick, D., Schmedding, E., De Vriendt, E., Jacobs, A. et al. (2003). Mutations in the small GTP-ase late endosomal protein RAB7 cause Charcot-Marie-Tooth type 2B neuropathy. *Am. J. Hum. Genet.* **72**, 722-727.

Weterman, M. A., Sorrentino, V., Kasher, P. R., Jakobs, M. E., van Engelen, B. G., Fluiter, K., de Wissel, M. B., Sizarov, A., Nurnberg, G., Nurnberg, P. et al. (2012). A frameshift mutation in LRSAM1 is responsible for a dominant hereditary polyneuropathy. *Hum. Mol. Genet.* **21**, 358-370.

Wooley, C. M., Sher, R. B., Kale, A., Frankel, W. N., Cox, G. A. and Seburn, K. L. (2005). Gait analysis detects early changes in transgenic SOD1(G93A) mice. *Muscle Nerve* **32**, 43-50.

Wooley, C. M., Xing, S., Burgess, R. W., Cox, G. A. and Seburn, K. L. (2009). Age, experience and genetic background influence treadmill walking in mice. *Physiol. Behav.* **96**, 350-361.

Xie, W., Li, L. and Cohen, S. N. (1998). Cell cycle-dependent subcellular localization of the TSG101 protein and mitotic and nuclear abnormalities associated with TSG101 deficiency. *Proc. Natl. Acad. Sci. USA* **95**, 1595-1600.

Zhang, Y., Zolov, S. N., Chow, C. Y., Slutsky, S. G., Richardson, S. C., Piper, R. C., Yang, B., Nau, J. J., Westrick, R. J., Morrison, S. J. et al. (2007). Loss of Vac14, a regulator of the signaling lipid phosphatidylinositol 3,5-bisphosphate, results in neurodegeneration in mice. *Proc. Natl. Acad. Sci. USA* **104**, 17518-17523.

Zhong, Q., Chen, Y., Jones, D. and Lee, W. H. (1998). Perturbation of TSG101 protein affects cell cycle progression. *Cancer Res.* **58**, 2699-2702.

Zhu, Q., Couillard-Després, S. and Julien, J. P. (1997). Delayed maturation of regenerating myelinated axons in mice lacking neurofilaments. *Exp. Neurol.* **148**, 299-316.

Disease Models & Mechanisms • DMM